

Delayed Electron–Ion Entanglement Revealed with Zero Area Pulses

Axel Stenquist and Jan Marcus Dahlström[†]
Department of Physics, Lund University, 22100 Lund, Sweden.

The Grobe–Eberly doublet phenomenon occurs in photoelectron distributions when the remaining ion is dressed by a field. As was recently shown, the doublet can be interpreted as a signature of quantum entanglement between photoelectrons and strongly coupled ions. However, the dressed state nature of the ion prevents detection of the entanglement by straightforward coincidence detection. Here, we find that odd (zero-area) envelopes can substantially delay the generation of entanglement, but also modify the dynamics such that the doublet transforms into unique channel-resolved photoelectron distributions. Because these distributions can be used to correlate with the internal state of the ion, our proposed scheme opens up for detection of quantum entanglement, between photoelectrons and strongly-coupled ions, without a need for quantum phase measurements.

A curious feature of zero-area pulses is that they induce transient dynamics in a two-level system, but eventually return the system to its initial state. First discovered half a century ago, in the context of propagating light pulses, through theoretical investigations [1–4] and subsequently confirmed by experimental investigations [5, 6], zero-area pulses are now a well-known concept in quantum control theory [7]. Though resonant zero-area pulses, acting like solitons, leave the system unchanged, population transfer in two-level systems can be achieved by using detuned or chirped pulses [7–9]. Over the last decades, pulse reshaping through atomic/molecular medium has moved from picosecond [10] to femtosecond timescales [11]. Recently, the generation of zero-area pulses in perfect transient absorption with attosecond pulses was reported [12]. Zero-area pulses have also been used in single-photon physics, with applications in quantum information processing [13, 14], where phase information has been retrieved with holographic, coincidence measurements [15].

Quantum entanglement and decoherence between massive particles created through the photoelectric effect have been performed using synchrotron radiation with coincidence detection [16, 17], and more recently with time-resolution provided by attosecond pulses [18–21], in atoms and small molecules. The theory of entanglement in ultrafast light-driven processes is a rapidly expanding subject [22–28]. The development of free-electron lasers (FEL) enables production of high-intensity ultrashort pulses in the extreme-ultraviolet (XUV) and X-ray regime that are utilized in a multitude of unique strong-field investigations [29–33]. Seeded FELs, such as FERMI [34], additionally provide temporal coherence, allowing for coherent control experiments [35–37]. In particular, seeded FELs allow for strong coupling at XUV wavelengths [38], which is essential for quantum operations on ultrafast timescales. Recently an investigation of quantum entanglement in the photoelectric effect, generated between photoelectrons and light-dressed atomic

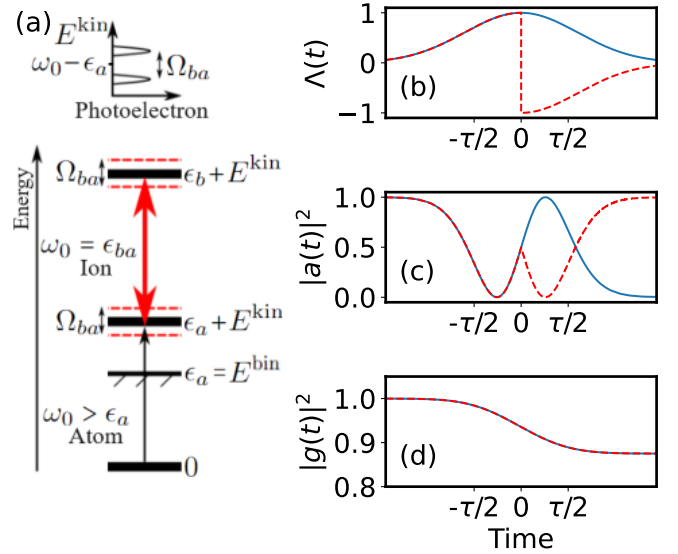


Figure 1. *Grobe–Eberly doublet formation and dynamics of Gaussian and zero-Gaussian pulses.* (a) Schematic illustrating the formation of the Grobe–Eberly doublet due to the dressing of the ion. (b) Pulse envelope for a Gaussian, $\Lambda_{\tau}^{\text{even}}(t)$, (blue) and zero-Gaussian pulse, $\Lambda_{\tau}^{\text{zero}}(t)$, (red dashed). The corresponding Rabi dynamics in the ionic ground state population $|a(t)|^2$ are presented in (c). The population of the atomic ground state $|g(t)|^2$ is presented in (d).

ions, was conducted at FERMI [39]. In agreement with the seminal theoretical work of Grobe and Eberly [40], and more recent investigations [41–44], a doublet was observed in the photoelectron spectrum corresponding to two dressed states of the ion, as illustrated in Fig. 1(a). The final state is not factorizable:

$$|\Psi\rangle \sim |+\rangle \otimes |\epsilon_{-}\rangle + |-\rangle \otimes |\epsilon_{+}\rangle \neq |\Psi_{\text{ion}}\rangle \otimes |\Psi_e\rangle, \quad (1)$$

due to different photoelectron energies, ϵ_{\mp} , being associated to the two dressed ion states, $|\pm\rangle \sim |a\rangle \pm i|b\rangle$. While the physical mechanism for this effect was attributed to quantum entanglement [39], its degree could not be measured. In fact, it would require coincidence detection of the photoelectron and ion with simultaneous quantum

[†] marcus.dahlstrom@matfys.lth.se

phase measurements — a task beyond current capabilities.

In this letter, we propose that a special class of zero-area pulses significantly reduce the complexity of detecting quantum entanglement between photoelectrons and ions in the strong-coupling regime. As we compare our results of regular and zero-area pulses, we find that: i) the generation of entanglement can be delayed and ii) the photoelectron distributions change so that electrons coupled to different ionic states avoid each other, which opens up for coincidence detection of entanglement. Atomic units are used throughout this text, $e = \hbar = m_e = 4\pi\epsilon_0 = 1$, unless otherwise stated.

Theory: Electron dynamics are computed semi-classically, within the dipole approximation, driven by a time-dependent electric field, $E(t) = E_0\Lambda_\tau(t)\sin(\omega_0 t)$, where E_0 , $\Lambda_\tau(t)$ and ω_0 is the amplitude, envelope and central frequency of the field, respectively. Additionally, τ denotes the full width at half max of the squared envelope. In resonant interactions with two-level atoms, the interaction amplitudes: $a(t) = \cos[\theta(t)/2]$ and $b(t) = \sin[\theta(t)/2]$, follow the pulse area $\theta(t) = \int^t \Omega(t')dt'$ [45], where $\Omega(t) = z_{ba}E_0\Lambda_\tau(t) \in \mathbb{R}$ is the Rabi frequency coupling the ground state $|a\rangle$ to the excited state $|b\rangle$, through the dipole matrix element, z_{ba} . It is useful to define the *absolute* pulse area for the total envelope: $\theta_\tau = \int_{-\infty}^{\infty} dt|\Omega(t)|$, as well as the *effective* Rabi frequency: $\bar{\Omega} = \int dt|\Omega(t)|^3 / \int dt|\Omega(t)|^2$, for pulses with general envelopes.

Zero-area envelopes.— The defining property of zero-area pulses is that they have a vanishing area at the end of the pulse: $\lim_{t \rightarrow \infty} \theta(t) = 0$. Clearly, any integrable odd function, $\Lambda_\tau^{\text{odd}}(t) = -\Lambda_\tau^{\text{odd}}(-t)$, satisfies this condition. In contrast, envelopes used to describe pulses in experiments are often positive even functions, $\Lambda_\tau^{\text{even}}(t) = \Lambda_\tau^{\text{even}}(-t) \geq 0$, as example Gaussian or flat-top pulses. Positive area pulses can rotate the initial state on the Bloch sphere by the angle $\theta(t)$ [46]. Here, we consider a special class of zero-area pulses generated from even functions as $\Lambda_\tau^{\text{zero}}(t) = \text{sign}(t)\Lambda_\tau^{\text{even}}(t)$. In particular, we will study the Gaussian and its corresponding zero-area envelope, the "zero Gaussian", but our conclusions are generally applicable to other envelopes. Qualitatively similar results are also expected for smooth sign changes [7]. A comparison of the 3π -area Gaussian envelope and its corresponding zero-area envelope is presented in Fig. 1(b). The Gaussian pulse causes Rabi flopping to the excited state, while the zero-area pulse induces a time reversal of the dynamics at the centre of the pulse, bringing the population back to the ground state, as shown in Fig. 1(c). Clearly, the atomic the populations, $|a(t)|^2$ and $|b(t)|^2 = 1 - |a(t)|^2$, are even functions for odd envelope pulses. The interaction amplitudes are also even functions, as is evident from their area dependence.

In contrast to the two-level system, the photoelectric effect is Markovian, and the ionization rate is unaffected by a sudden sign change of the envelope. In Fig. 1(d), we show that the survival probability of the atomic ground state, driven by Gaussian and zero-Gaussian pulses, are indeed identical. This is easily understood from the instantaneous photoionization rate: $\Gamma_{ag}(t) = 2\pi|z_{ag}E_0\Lambda_\tau(t)/2|^2$, which depends only on the square of the envelope and the coupling to the continuum, z_{ag} .

Grobe–Eberly doublet.— The photoelectric effect predicts that the kinetic energy of the photoelectron is $E^{\text{kin}} = \omega_0 - E^{\text{bin}}$, where E^{bin} is the binding energy of the helium atom. However, in the presence of a strongly coupled ionic resonance, Grobe and Eberly predicted a modification to this effect with the formulation of a doublet due to the dressing of the ion by the field [40], with peaks separated by the Rabi frequency. We define the relative photoelectron energy, $\epsilon = E^{\text{kin}} - (\omega_0 - E^{\text{bin}})$, the photoelectron peaks then appear at the energies $\epsilon_\pm = \pm\bar{\Omega}/2$, corresponding to two final dynamically dressed ionic states.

The dynamics can be explained using a 2-step model: i) the field ionizes the atom at time t , by the interaction: $z_{ag}E_0\Lambda_\tau(t)/2$, leaving the ion in the ground state a and creating a photoelectron with the remaining energy ϵ . ii) the field induces Rabi oscillations in the ion between the ground and excited state, $j_\tau(-t)$, where $j \in \{a, b\}$, while the photoelectron propagates freely, $e^{i\epsilon t}$. This analytical model describes the dynamically dressed ion, yielding the final state amplitudes of the ion and photoelectron

$$c_j(\tau, \epsilon) = \frac{\Omega_0^{ag}}{2} \int_{-\infty}^{\infty} dt j_\tau(-t)\Lambda_\tau(t)g_\tau(t)e^{i\epsilon t}, \quad (2)$$

where $j_\tau(t)$ and $g_\tau(t)$ are ionic and atomic interaction amplitudes, respectively. The final-state full density matrix can then be constructed from $\rho_{gg}(\tau) = g_\tau^*(\infty)g_\tau(\infty)$, $\rho_{gj}(\tau; \epsilon) = g_\tau^*(\infty)c_j(\tau, \epsilon)$ and $\rho_{jj'}(\tau; \epsilon, \epsilon') = c_j^*(\tau, \epsilon)c_{j'}(\tau, \epsilon')$, as described in the supplemental material [47].

Results: We consider the experimentally relevant helium photoionization process, assuming the dipole matrix element $z_{ag} = 0.502$ to be constant for the relevant photoelectron energies. The field is resonant with the ionic transition between 1s and 2p, with the dipole matrix element $z_{ba} = 0.373$, and the resonant energy $\omega_0 = \epsilon_b - \epsilon_a = 40.2$ eV. The peak intensity of the Gaussian and zero-Gaussian envelopes is set to $I_0 = 1.25 \cdot 10^{13}$ W/cm², corresponding to a maximum Rabi frequency of $\Omega_0 = z_{ba}E_0 \approx 0.2$ eV, and an effective Rabi frequency of $\bar{\Omega} \approx 0.16$ eV. Pulse durations, τ , up to 81 fs are considered, corresponding to absolute pulse areas $0 \leq \theta_\tau \leq 10\pi$. First, we present the ion dynamics $\int |c_j(\tau, \epsilon)|^2 d\epsilon$, followed by the photoelectron spectrum $|c_a(\tau, \epsilon)|^2 + |c_b(\tau, \epsilon)|^2$, where $|c_a(\tau, \epsilon)|^2$ and $|c_b(\tau, \epsilon)|^2$ are the ion-channel resolved photoelectron probability distributions for the ground and excited state, respectively.

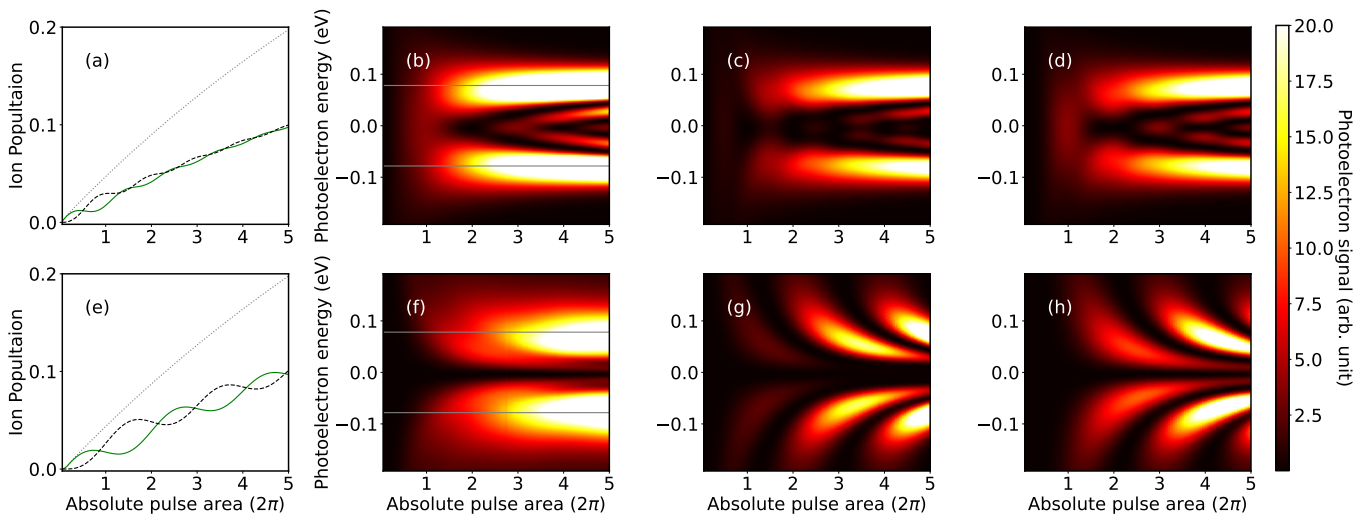


Figure 2. *Build-up of the ion dynamics and photoelectron spectra over absolute pulse area, at constant peak intensity.* **Top row:** presents results for Gaussian pulses. (a) shows the ion populations of the ground state (green), the excited state (black dashed) and the full ionic population (grey dotted). The photoelectron probability distribution is presented in (b) and the ion-channel-resolved photoelectron spectra corresponding to the ground state and excited state channels are presented in (c) and (d), respectively. **Bottom row:** presents the corresponding results for the zero-Gaussian pulse. Heat maps are saturated at high photoelectron signals.

Ion dynamics.— For a Gaussian pulse, we observe oscillations in the ionic state populations as the pulse area is increased, as presented in Fig. 2(a). In contrast to the flat-top case presented in [39, 43, 44], the oscillations are attenuated with increasing pulse area, presumably due to the range of instantaneous intensities. The oscillations are not aligned with the pulse area, but the number of Rabi periods approximately agrees with the expected five Rabi periods at the end of the pulse. In contrast, we find that for the zero-Gaussian pulse, Fig. 2(e) the ion goes through half the number of oscillations, 2.5 Rabi periods, and shows less clear signs of attenuation.

Photoelectron spectra.— In Fig. 2(b), we present the pulse-area-resolved final-state photoelectron spectra for Gaussian pulses. The spectra develop from a single peak, centred on the resonant photoelectron energy, $\epsilon = 0$, to the dynamical Grobe–Eberly doublet, $\pm\Omega/2$ (grey lines). Dynamic substructures between the peaks, related to the number of completed Rabi cycles, are observed [43]. The channel-resolved photoelectron spectra are presented in (c) and (d) for the ionic ground and excited state, respectively. The doublet forms earlier in the ground state, around one Rabi period $\theta = 2\pi$, whereas in the excited state, it forms at $\theta = 3\pi$ [44].

In Fig. 2(f), we show that zero-Gaussian pulses yield photoelectron distributions that differ subtly from the dynamical Grobe–Eberly doublet phenomenon. Firstly, no peak is formed at the energy $\epsilon = 0$, which means that the usual photoelectric pathway is “blocked”. Secondly, the photoelectron spectra for larger areas form a doublet with significantly wider peaks. Thirdly, the dy-

namic interference structure between the doublet peaks is missing. The difference between Gaussian and zero-Gaussian pulses is more striking in the channel-resolved photoelectron distributions. The two channels do not overlap, as observed in (g) and (h) corresponding to the ground and excited state, respectively. These novel behaviours are due to the symmetries associated with the zero-area pulses, as will be discussed below.

Discussion: While even envelopes form dynamically dressed states, the odd envelopes do not allow for well-defined dressed states to be formed. Therefore, different electron distributions will be generated with unique properties caused by the odd envelope symmetry.

For the zero-Gaussian pulse, the central peak does not form at $\epsilon = 0$. This is clear from Eq. (2) since the depletion is small, $g_\tau(t) \approx 1$, the envelope, $\Lambda_\tau^{\text{zero}}(t)$, is odd and the state amplitudes, $j_\tau(t)$, are even for all pulse durations. Hence, the integrand is zero, inhibiting resonant photoionization. An analytical expression for the final state amplitudes in the zero-area-pulse case can be determined for the flat-top envelope by neglecting depletion, as $c_j = c_j^+ + c_j^-$,

$$c_a^\pm(\tau, \epsilon) = \frac{i\Omega_0^{ag} \cos(\epsilon\tau/2) \pm \cos(\Omega_0\tau/4)}{2 \Omega_0/2 \mp \epsilon},$$

$$c_b^\pm(\tau, \epsilon) = -\frac{i\Omega_0^{ag} \sin(\epsilon\tau/2) \mp \sin(\Omega_0\tau/4)}{2 \Omega_0/2 \mp \epsilon},$$
(3)

where the origin of the doublet peaks is observed, centred on $\pm\Omega_0/2$. The photoelectron densities of the two channels avoid each other, as they are of cosine and sine character for the ionic ground and excited state, respec-

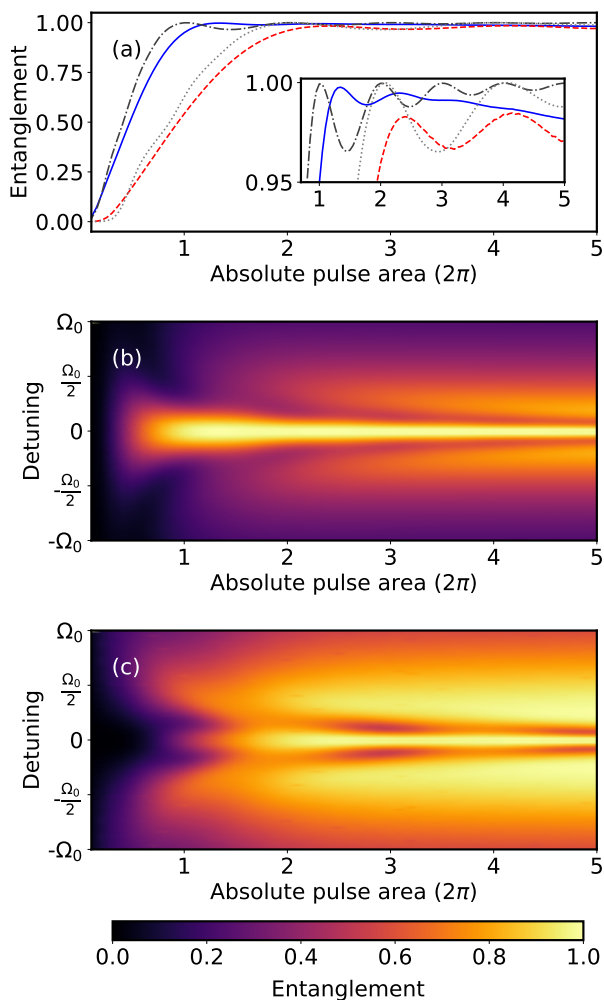


Figure 3. *Entanglement resolved over pulse area and detuning.* Absolute-pulse-area resolved entanglement (a) for a resonant Gaussian (blue) and its corresponding zero-area pulse (red dashed) as well as a flat top (dark grey dash-dotted) and flat-top zero-area pulse (light grey dotted). Detuning- and pulse-area-resolved entanglement is presented in (b) and (c) for the Gaussian and zero-Gaussian pulses, respectively.

tively. By comparing with the analytical model for the flat-top pulse, we note that the even pulse yields oscillations at twice the frequency of the zero area pulse, as observed in Fig. 2 and Fig. 3. See the supplemental material [47] for details on the analytical models.

Entanglement.— In order to analyse our results, we form the post-measurement density matrix by conditioning the full density matrix on the photoionization, by applying the ion-space projection operator $Q = \int d\epsilon \sum_j |j, \epsilon\rangle \langle j, \epsilon|$ and renormalizing with the ion-space population, $\text{Tr}\{\rho Q\}$. The post-measurement density matrix is then $\tilde{\rho} = Q\rho Q / \text{Tr}\{\rho Q\} = \sum_{jj'} \iint d\epsilon d\epsilon' \rho'_{jj'}(\tau; \epsilon, \epsilon') |j, \epsilon\rangle \langle j', \epsilon'|$. The degree of entanglement is quantified using the Von Neumann entropy of entanglement $S(\tau) = -\text{Tr}\{\rho^I(\tau) \log_2[\rho^I(\tau)]\}$, where

$\rho^I(\tau) = \text{Tr}_e\{\tilde{\rho}(\tau)\}$ is the 2×2 reduced density matrix of the ion [48]. The entanglement, resolved over pulse area, is presented in Fig. 3(a) for the Gaussian and zero-Gaussian pulse. Additionally, the flat-top envelope entanglements are given. The insert shows the entanglement between 0.95 and 1. Compared to the flat-top pulses, we see a slight delay in the build-up of entanglement for smooth pulses. In contrast, the entanglement is severely delayed in the case of zero-area pulses, where the flat top becomes fully entangled at $\theta = 4\pi$ and the zero-area Gaussian is slightly further delayed. The entanglement can be understood by the simplified wave function:

$$|\Psi_{zero}\rangle \rightarrow |a\rangle \otimes |E_a^{\text{kin}}\rangle + |b\rangle \otimes |E_b^{\text{kin}}\rangle \neq |\Psi_{\text{ion}}\rangle \otimes |\Psi_e\rangle, \quad (4)$$

where the internal states of the ion correlate with different kinetic energies, $E_a^{\text{kin}} \neq E_b^{\text{kin}}$, as shown in Fig. 2(g) and (h).

Detuning.— By introducing a detuning to the pulse, $\omega_0 = \epsilon_b - \epsilon_a + \Delta\omega$, we can change the dynamical build-up of the entanglement. Detuning- and absolute-pulse-area-resolved entanglement is shown in Fig. 3(b) and (c) for the Gaussian and its corresponding zero-area pulse, respectively. In the Gaussian pulse case, the entanglement decreases with detuning, showing minor wings near resonance. In contrast, in the zero-Gaussian pulse case, the entanglement develops later in the resonant case than in the detuned case with strong wings.

Conclusions: In this letter, we have studied the entanglement between photoelectrons and strongly coupled ions. Our results show that odd envelopes, which are a special class of zero-area pulses, break the dressing mechanism of the ion and alter the photoelectron distribution. The resonant photoelectric effect is blocked and entanglement is delayed by a factor of two in terms of absolute pulse area. Despite the breakdown of dressed states, induced by zero-area pulses, the entanglement eventually reaches values close to those maximally allowed for qubit systems, but its manifestation is changed: the electrons now avoid each other when detected in coincidence with the internal states of the ion Fig. 2(g,h). Thus, our work provides key insights for future pump-probe experiments on the entanglement between electrons and coupled states of ions [23, 26, 44].

ACKNOWLEDGEMENTS

We acknowledge fruitful discussions with Edvin Olofsson and Yijie Liao. JMD acknowledges support from the Olle Engkvist Foundation: 194-0734 and the Knut and Alice Wallenberg Foundation: 2019.0154.

-
- [1] C. K. Rhodes, A. Szöke, and A. Javan, The Influence of Level Degeneracy on the Self-Induced Transparency Effect, *Phys. Rev. Lett.* **21**, 1151 (1968).
- [2] D. C. Burnham and R. Y. Chiao, Coherent Resonance Fluorescence Excited by Short Light Pulses, *Phys. Rev.* **188**, 667 (1969).
- [3] M. D. Crisp, Propagation of Small-Area Pulses of Coherent Light through a Resonant Medium, *Phys. Rev. A* **1**, 1604 (1970).
- [4] F. A. Hopf, G. L. Lamb, C. K. Rhodes, and M. O. Scully, Some Results on Coherent Radiative Phenomena with 0π Pulses, *Phys. Rev. A* **3**, 758 (1971).
- [5] H. Grieneisen, J. Goldhar, N. Kurnit, A. Javan, and H. Schlossberg, Observation of the transparency of a resonant medium to zero-degree optical pulses, *Applied Physics Letters* **21**, 559 (1972).
- [6] S. M. Hamadani, J. Goldhar, N. A. Kurnit, and A. Javan, Coherent optical pulse reshaping in a resonant molecular absorber, *Applied Physics Letters* **25**, 160 (1974).
- [7] G. S. Vasilev and N. V. Vitanov, Complete population transfer by a zero-area pulse, *Phys. Rev. A* **73**, 023416 (2006).
- [8] J. M. S. Lehto and K.-A. Suominen, Time-dependent two-level models and zero-area pulses, *Phys. Scr.* **91**, 013005 (2016).
- [9] H.-g. Lee, Y. Song, H. Kim, H. Jo, and J. Ahn, Quantum dynamics of a two-state system induced by a chirped zero-area pulse, *Phys. Rev. A* **93**, 023423 (2016).
- [10] J. E. Rothenberg, D. Grischkowsky, and A. C. Balant, Observation of the Formation of the 0π Pulse, *Phys. Rev. Lett.* **53**, 552 (1984).
- [11] M. Matusovsky, B. Vaynberg, and M. Rosenbluh, 0π pulse propagation in the extreme sharp-line limit, *J. Opt. Soc. Am. B* **13**, 1994 (1996).
- [12] Y. He, Z. Liu, C. Ott, A. N. Pfeiffer, S. Sun, M. B. Gaarde, T. Pfeifer, and B. Hu, Resonant Perfect Absorption Yielded by Zero-Area Pulses, *Phys. Rev. Lett.* **129**, 273201 (2022).
- [13] S. Derouault and M. Bouchene, One-photon wavepacket interacting with a two-level atom in a waveguide: Constraint on the pulse shape, *Physics Letters A* **376**, 3491 (2012).
- [14] L. Costanzo, A. Coelho, D. Pellegrino, M. Mendes, L. Acioli, K. Casemiro, D. Felinto, A. Zavatta, and M. Bellini, Zero-Area Single-Photon Pulses, *Phys. Rev. Lett.* **116**, 023602 (2016).
- [15] M. Lipka and M. Parniak, Single-Photon Hologram of a Zero-Area Pulse, *Phys. Rev. Lett.* **127**, 163601 (2021).
- [16] D. Akoury *et al.*, The Simplest Double Slit: Interference and Entanglement in Double Photoionization of H₂, *Science* **318**, 949 (2007).
- [17] M. N. Piancastelli, R. Guillemin, T. Marchenko, L. Journel, O. Travnikova, T. Marin, G. Goldsztejn, B. C. De Miranda, I. Ismail, and M. Simon, New achievements on relaxation dynamics of atoms and molecules photoexcited in the tender x-ray domain at synchrotron SOLEIL, *J. Phys. B: At. Mol. Opt. Phys.* **50**, 042001 (2017).
- [18] T. Nishi, E. Lötstedt, and K. Yamanouchi, Entanglement and coherence in photoionization of H₂ by an ultrashort XUV laser pulse, *Phys. Rev. A* **100**, 013421 (2019).
- [19] M. J. Vrakking, Control of Attosecond Entanglement and Coherence, *Phys. Rev. Lett.* **126**, 113203 (2021).
- [20] D. Busto *et al.*, Probing electronic decoherence with high-resolution attosecond photoelectron interferometry, *Eur. Phys. J. D* **76**, 112 (2022).
- [21] L.-M. Koll, L. Maikowski, L. Drescher, T. Witting, and M. J. Vrakking, Experimental Control of Quantum-Mechanical Entanglement in an Attosecond Pump-Probe Experiment, *Phys. Rev. Lett.* **128**, 043201 (2022).
- [22] M. V. Fedorov, M. A. Efremov, A. E. Kazakov, K. W. Chan, C. K. Law, and J. H. Eberly, Packet narrowing and quantum entanglement in photoionization and photodissociation, *Phys. Rev. A* **69**, 052117 (2004).
- [23] J.-A. You, N. Rohringer, and J. M. Dahlström, Attosecond photoionization dynamics with stimulated core-valence transitions, *Phys. Rev. A* **93**, 033413 (2016).
- [24] M. Ruberti, S. Patchkovskii, and V. Averbukh, Quantum coherence in molecular photoionization, *Phys. Chem. Chem. Phys.* **24**, 19673 (2022).
- [25] A. S. Maxwell, L. B. Madsen, and M. Lewenstein, Entanglement of orbital angular momentum in non-sequential double ionization, *Nat Commun* **13**, 4706 (2022).
- [26] K. L. Ishikawa, K. C. Prince, and K. Ueda, Control of Ion-Photoelectron Entanglement and Coherence Via Rabi Oscillations, *J. Phys. Chem. A* **127**, 10638 (2023).
- [27] M. Ruberti, V. Averbukh, and F. Mintert, Bell test of quantum entanglement in attosecond photoionization 10.48550/ARXIV.2312.05036 (2023), publisher: [object Object] Version Number: 2.
- [28] P. Stammer, J. Rivera-Dean, A. Maxwell, T. Lamprou, A. Ordóñez, M. F. Ciappina, P. Tzallas, and M. Lewenstein, Quantum Electrodynamics of Intense Laser-Matter Interactions: A Tool for Quantum State Engineering, *PRX Quantum* **4**, 010201 (2023).
- [29] L. Young *et al.*, Femtosecond electronic response of atoms to ultra-intense X-rays, *Nature* **466**, 56 (2010).
- [30] E. Lindroth, F. Calegari, L. Young, M. Harmand, N. Dudovich, N. Berrah, and O. Smirnova, Challenges and opportunities in attosecond and XFEL science, *Nat Rev Phys* **1**, 107 (2019).
- [31] L. Young *et al.*, Roadmap of ultrafast x-ray atomic and molecular physics, *J. Phys. B: At. Mol. Opt. Phys.* **51**, 032003 (2018).
- [32] A. Rudenko *et al.*, Femtosecond response of polyatomic molecules to ultra-intense hard X-rays, *Nature* **546**, 129 (2017).
- [33] E. P. Kanter *et al.*, Unveiling and Driving Hidden Resonances with High-Fluence, High-Intensity X-Ray Pulses, *Phys. Rev. Lett.* **107**, 233001 (2011).
- [34] E. Allaria *et al.*, Highly coherent and stable pulses from the FERMI seeded free-electron laser in the extreme ultraviolet, *Nature Photon* **6**, 699 (2012).
- [35] M. Fushitani, C.-N. Liu, A. Matsuda, T. Endo, Y. Toida, M. Nagasono, T. Togashi, M. Yabashi, T. Ishikawa, Y. Hikosaka, T. Morishita, and A. Hishikawa, Femtosecond two-photon Rabi oscillations in excited He driven by ultrashort intense laser fields, *Nature Photon* **10**, 102 (2016).
- [36] K. C. Prince *et al.*, Coherent control with a short-wavelength free-electron laser, *Nature Photon* **10**, 176 (2016).
- [37] P. K. Maroju *et al.*, Attosecond coherent control of electronic wave packets in two-colour photoionization using a novel timing tool for seeded free-electron laser, *Nat.*

- Photon. **17**, 200 (2023).
- [38] S. Nandi *et al.*, Observation of Rabi dynamics with a short-wavelength free-electron laser, *Nature* **608**, 488 (2022).
- [39] S. Nandi *et al.*, Generation of entanglement using a short-wavelength seeded free-electron laser, *Sci. Adv.* **10**, eado0668 (2024).
- [40] R. Grobe and J. H. Eberly, Observation of coherence transfer by electron-electron correlation, *Phys. Rev. A* **48**, 623 (1993).
- [41] B. Walker, M. Kaluža, B. Sheehy, P. Agostini, and L. F. DiMauro, Observation of Continuum-Continuum Autler-Townes Splitting, *Phys. Rev. Lett.* **75**, 633 (1995).
- [42] L. G. Hanson, J. Zhang, and P. Lambropoulos, Manifestations of atomic and core resonances in photoelectron energy spectra, *Phys. Rev. A* **55**, 2232 (1997).
- [43] S. B. Zhang and N. Rohringer, Photoemission spectroscopy with high-intensity short-wavelength lasers, *Phys. Rev. A* **89**, 013407 (2014).
- [44] C. Yu and L. B. Madsen, Core-resonant ionization of helium by intense XUV pulses: Analytical and numerical studies on channel-resolved spectral features, *Phys. Rev. A* **98**, 033404 (2018).
- [45] S. L. McCall and E. L. Hahn, Self-Induced Transparency by Pulsed Coherent Light, *Phys. Rev. Lett.* **18**, 908 (1967).
- [46] R. P. Feynman, F. L. Vernon, and R. W. Hellwarth, Geometrical Representation of the Schrödinger Equation for Solving Maser Problems, *Journal of Applied Physics* **28**, 49 (1957).
- [47] See Supplemental Material [url] for details on the theoretical methods and the physical phenomena investigated,.
- [48] S. Haroche and J.-M. Raimond, *Exploring the quantum: atoms, cavities, and photons*, first published in paperback ed., Oxford graduate texts (Oxford University Press, Oxford, 2013).